Algebraic Signal Processing Theory: 2-D Spatial Hexagonal Lattice

Markus Püschel, *Senior Member, IEEE,* and Martin Rötteler, *Member, IEEE*

***Abstract*—We develop the framework for signal processing on a spatial, or undirected, 2-D hexagonal lattice for both an infinite and a finite array of signal samples. This framework includes the proper notions of z-transform, boundary conditions, filtering or convolution, spectrum, frequency response, and Fourier transform. In the finite case, the Fourier transform is called discrete triangle transform (DTT). Like the hexagonal lattice, this transform is nonseparable. The derivation of the framework makes it a natural extension of the algebraic signal processing theory that we recently introduced. Namely, we construct the proper signal models, given by polynomial algebras, bottom-up from a suitable definition of hexagonal space shifts using a procedure provided by the algebraic theory. These signal models, in turn, then provide all the basic signal processing concepts. The framework developed in this paper is related to Mersereau's early work on hexagonal lattices in the same way as the discrete cosine and sine transforms are related to the discrete Fourier transform—a fact that will be made rigorous in this paper.**

***Index Terms*—Discrete triangle transform, polynomial algebra, Chebyshev polynomials in two variables, nonseparable, discrete cosine transform, representation theory, convolution, spectrum**

I. Introduction

It is well-known that applying a 2-D discrete Fourier transform (DFT) to an $n \times n$ set of signal values implicitly places it on a square array with cyclic boundary conditions and a periodic signal extension. Further, the array is directed because of the availability of shifts in both dimensions (see Fig. 1(a)). Similarly, and less well-known, for the 2-D discrete cosine and sine transforms (DCTs and DSTs), the signal is again placed on a square array, but this time the boundary conditions are symmetric or antisymmetric (depending on the type of DCT or DST) [1] and the array is undirected (see Fig. 1(b)). Intuitively, this property makes these transforms more suitable for spatial[1] signals, i.e., signals without inherent direction, like images.

In this paper, we develop the framework for signal processing on an undirected or spatial hexagonal lattice extending our preliminary work [2]. We consider both the case of an infinite hexagonal lattice and of a finite array shown in Fig. 1(c). In particular, for the latter, we introduce the proper 2-D spectral transform, which we call discrete triangle transform (DTT). Since the array in Fig. 1(c) is nonseparable the DTT is not a Kronecker product of 1-D transforms.

We develop the signal processing on a spatial hexagonal lattice as an application and natural extension of the algebraic signal processing theory—a general approach to linear signal processing introduced in [3], [4], [5]. In particular, we introduced in [3] a bottom-up procedure to derive signal processing frameworks, called signal models, from basic principles, namely from a suitable definition of the shift operator. We will apply this procedure to suitably chosen hexagonal space shifts to derive for the hexagonal lattice the sensible choices of boundary conditions and signal extension, the proper notion of associated "z-transform," filtering or convolution, as well as spectrum, frequency response, Fourier transform, and its diagonalization properties. In the finite case, the Fourier transform is exactly the DTT, of which we derive two variants.

Equally important as the results is the actual derivation, which we will show to parallel in many ways the derivation of the signal models underlying the DCTs/DSTs [5]. Examples of parallels include the best choices of boundary conditions and the occurrence of Chebyshev polynomials in one and two variables, respectively. For this reason, and to make the paper as self-contained as possible, we first spend some time on introducing the relevant parts of the algebraic signal processing theory including the derivation of the signal processing framework associated with the DCTs and DSTs.

The DTT also possesses fast Cooley-Tukey FFT type algorithms that puts it in the same complexity class as its separable counterparts [6]. These algorithms are also derived using the algebraic theory, namely through a 2-D extension of the methods used in [7] to derive DFT, DCT, and DST algorithms. A detailed version of [6] will serve as second part [8] to the present paper.

Related work. Signal processing, in particular the proper forms of spectral analysis, on an infinite and finite hexagonal lattice has been studied to great detail in the seminal paper of Mersereau [9] as application of his general theory of multi-dimensional signal processing [10]. However, the lattices considered by Mersereau are directed, i.e., are of the type shown in Fig. 1(a) in contrast to Fig. 1(b) and (c). In other words, the relationship between this paper and [9] is the same as between signal processing using the DCTs/DSTs and using the DFT.

Several papers deal with the question of speeding-up the computation of Mersereau's definition of a hexagonal DFT; see [11] and the references given therein. The problem of resampling from Cartesian to hexagonal coordinates was considered in [12]. Splines for hexagonal lattices were introduced in [13].

A more extensive treatment of hexagonal lattices in image

This work was supported by NSF through awards 0310941 and 0634967.

Markus Püschel is with the Department of Electrical and Computer Engineering, Carnegie Mellon University, 5000 Forbes Ave, Pittsburgh, PA 15213. E-mail: pueschel@ece.cmu.edu, phone: 412-268-3804, fax: 412-268-3890. Martin Rötteler is with NEC Laboratories America, Inc., 4 Independence Way, Suite 200, Princeton, NJ 08540. E-mail: mroetteler@nec-labs.com, phone: 609-951-2771

[1]In signal processing, the term "space" is often used for any type of 2-D processing; we use the term to distinguish undirected from directed signal processing. This distinction is made rigorous by the algebraic signal processing theory introduced later.

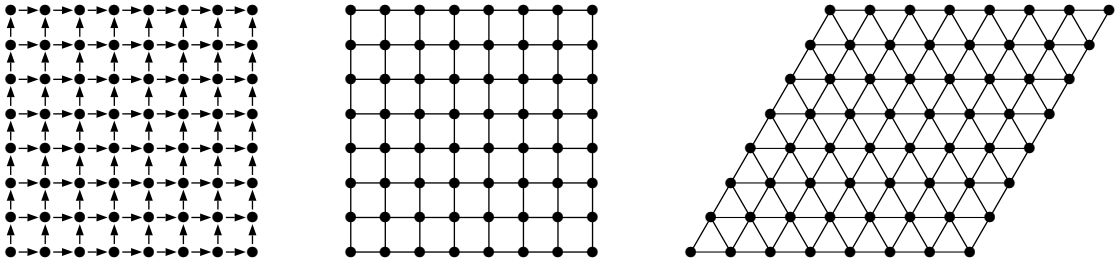

(a) 2-D DFT (b) 2-D DCT/DST (c) DTT

Fig. 1. Visualizations of the signal models underlying (a) the 2-D DFT (cyclic boundary conditions are omitted); (b) the 2-D DCTs/DSTs (symmetric/antisymmetric boundary conditions are omitted); and (c) the DTTs (boundary conditions are omitted) introduced in this paper.

processing and applications can be found in [14] and [15]: [14] discusses in detail halftoning techniques for rectangularly and hexagonally sampled images; [15] includes an up to date overview on the field of hexagonal image processing including applications and investigates in detail the difference to standard rectangular image processing. Regarding spectral analysis, both books built on the work of Mersereau, i.e., adopt directed signal models.

The only reference aiming to derive a DCT equivalent for hexagonal lattices appears to be [16]. However, the paper is very short and provides little insights in the presented transform, which is different from the ones derived here. It appears that [16] does not take all the six neighbor connections of a lattice point into account as we do by choosing the proper notions of shifts. Also, the actual transform is only a part of our contribution, which is a complete basic framework for spatial hexagonal signal processing.

Organization. The first three sections after this introduction provide background. In Section II we give a brief overview on the algebraic signal processing theory in the general case and then, to greater detail, in the special case of shift-invariant finite signal models, which require polynomial algebras as underlying structure. In Sections III and IV we sketch the derivation of the signal models for a spatial 1-D lattice. The derivation is structured to parallel the corresponding derivation of the 2-D hexagonal spatial signal models in Section V (infinite case) and Section VI (finite case). Section VII shows a small application example. Finally, we offer conclusions in Section VIII.

II. Algebraic Signal Processing Theory

The derivation of the signal processing framework for the 2-D spatial hexagonal lattice uses and makes it a natural part of the algebraic signal processing theory [3]. In this background section, we first introduce the general theory and, in particular, the concept of a signal model, which is central in this theory and the foundation for different ways of doing linear signal processing. Then we discuss to greater detail the special case of shift-invariant signal models in 1-D and 2-D. The latter provides the underpinning for signal processing on the spatial hexagonal lattice.

For details that exceed the scope of this paper, we refer the reader to [3].

A. Basic Concepts

The algebraic signal processing theory is a general framework for *linear* signal processing (henceforth simply called SP), i.e., signals are assumed to be elements of vector spaces and filters operate on signals as linear mappings. The crucial observation underlying the theory is that the structure in SP goes beyond vector spaces as explained next.

Filter space = algebra. An algebra is a vector space that is also a ring, i.e., it permits the multiplication of elements and the distributivity law holds. If we define in the space of filters (or SISO systems) multiplication as concatenation, then the filter space becomes an algebra. For example, in infinite discrete time SP, this algebra (in the z-domain) is given by[2]

$$\mathcal{A} = \{h = \sum_{n\in\mathbb{Z}} h_n z^{-n} \mid \mathbf{h} = (\dots, h_{-1}, h_0, h_1, \dots) \in \ell^1(\mathbb{Z})\}. \quad (1)$$

Note that we use bold-faced symbols like $\mathbf{h}$ to denote coordinate representations, i.e., sequences of scalars from the base field (assumed to be $\mathbb{C}$). The corresponding element of an algebra (or module below) is written unbolded like h.

Signal space = module. The signal space in SP is a vector space. Since filters operate as linear mappings on this space, it obtains additional structure, namely those of an $\mathcal{A}$-module, written as $\mathcal{M}$. In the infinite discrete time case, the module (also in the z-domain) commonly assumed is

$$\mathcal{M} = \{s = \sum_{n\in\mathbb{Z}} s_n z^{-n} \mid \mathbf{s} = (\dots, s_{-1}, s_0, s_1, \dots) \in \ell^2(\mathbb{Z})\}. \quad (2)$$

Signal model. Discrete signals arise in applications as sequences of numbers (e.g., after sampling) not as elements of modules. These sequences naturally form a vector space V. However, to have a notion of filtering and thus the associated notion of Fourier analysis, an algebra and a module have to be chosen or assigned. This is the purpose of the *signal model*, defined as a triple $(\mathcal{A}, \mathcal{M}, \Phi)$, where $\mathcal{A}$ is an algebra, $\mathcal{M}$ is an $\mathcal{A}$-module of the same dimension as V, and Φ is a one-to-one mapping from V to $\mathcal{M}$. As an example, the signal model

[2]Replacing ℓ^1 with ℓ^2 in (1) destroys the algebra structure: the concatenation of two ℓ^2 filters is in general not an ℓ^2 filter.

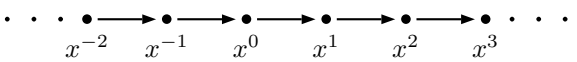

Fig. 2. Visualization of the infinite discrete time model (3).

adopted in infinite discrete time SP is given by $\mathcal{A}$ in (1), $\mathcal{M}$ in (2), and Φ is the z-transform

$$\Phi: \ \mathbf{s} = (\dots, s_{-1}, s_0, s_1, \dots) \mapsto s = \sum_{n\in\mathbb{Z}} s_n z^{-n}. \quad (3)$$

It is a model for finite-energy sequences $\mathbf{s} \in V = \ell^2(\mathbb{Z})$.

We call a model *regular* if $\mathcal{A} = \mathcal{M}$. The model (3) is not regular.

Once a model is chosen, filtering, Fourier analysis, and other concepts are automatically defined through the well-developed representation theory of algebras [3].

In discrete models, the shift operator(s) *generate* the algebras $\mathcal{A}$.[3] For example, (1) is generated by z^{-1}. A signal model is *shift-invariant* if and only if $\mathcal{A}$ is commutative. We *visualize* a model by letting the shift operator(s) operate on the basis b of $\mathcal{M}$ implicitly chosen through Φ (e.g., $b = (z^{-n})_{n\in\mathbb{Z}}$ in (3)) and by representing this operation as a graph. For example the discrete time model defined above is visualized in Fig. 2 (z^{-1} is replaced by x). Note that the graph is directed, which is intuitive, as it visualizes a time model. We will later encounter space models that have undirected visualizations.

B. Finite Shift-Invariant Signal Models in 1-D

In the previous section we have asserted that a shift invariant signal model $(\mathcal{A}, \mathcal{M}, \Phi)$ necessarily has a commutative algebra $\mathcal{A}$. If, in addition, the model is discrete and finite, i.e., for a finite number of samples, then $\mathcal{A}$ is a *polynomial algebra* [3]. Thus, polynomial algebras provide the underlying structure for many signal processing applications. Theory and many examples were developed in [3].

As necessary background for this paper, we introduce now polynomial algebras and the necessary properties of signal models built from them. We focus the discussion on the complex base field $\mathbb{C}$. Other base fields are handled analogously. Further, we start with the 1-D case, in which exactly one shift is available. The 2-D case (with two shifts) is discussed afterwards. As running example in this section, we use the signal model associated with the DFT.

Polynomial algebras (one variable). Let $p(x) \in \mathbb{C}[x]$ be a polynomial. A polynomial algebra (in one variable) is the set

$$\mathbb{C}[x]/p(x) = \{s(x) \in \mathbb{C}[x] \mid \deg(s) < \deg(p)\}.$$

Clearly, $\mathbb{C}[x]/p(x)$ is a vector space, but it is also an algebra if we define the multiplication of polynomials modulo the fixed polynomial $p(x)$. In the following, we require that $p(x)$ has pairwise distinct zeros denoted with $\alpha = (\alpha_0, \dots, \alpha_{n-1})$.

Signals models built from polynomial algebras. Assume $\mathbb{C}[x]/p(x)$ is given. Then we can build a regular signal model

[3]This means that every element in $\mathcal{A}$ is a polynomial or series in the shift operator(s).

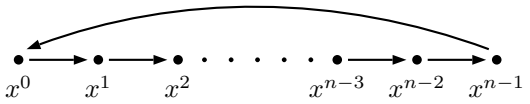

Fig. 3. Visualization of the finite discrete time model (5) for which the DFT is the Fourier transform.

for $V = \mathbb{C}^n$ by choosing a basis $b = (p_0, \dots, p_{n-1})$ and setting

$$\begin{aligned} &\mathcal{A} = \mathcal{M} = \mathbb{C}[x]/p(x), \\ &\Phi: \ \mathbb{C}^n \to \mathcal{M}, \ \mathbf{s} \mapsto s = s(x) = \textstyle\sum_{0\le\ell<n} s_\ell p_\ell(x). \end{aligned} \quad (4)$$

In (4), Φ is the "z-transform" and x is the shift (operator) that generates $\mathcal{A}$. Signals and filters in this model both are polynomials: $s(x) \in \mathcal{M}$ and $h(x) \in \mathcal{A}$. Filtering is the multiplication modulo $p(x)$

$$hs = h(x)s(x) \bmod p(x).$$

As an example,

$$\mathcal{A} = \mathcal{M} = \mathbb{C}[x]/(x^n - 1), \quad \Phi: \mathbf{s} \mapsto \sum_{0\le\ell<n} s_\ell x^\ell \quad (5)$$

defines a signal model. Filtering is multiplication of polynomials h and s modulo $x^n - 1$, which is equivalent to circular convolution of the coefficient vectors **h** and **s** [17]. For this reason, we call Φ the finite z-transform [4].

Filtering in coordinates. Every filter $h = h(x)$ is a linear mapping, and thus can be represented by a matrix M_h with respect to the basis b implicitly defined in the model (4). This defines a mapping

$$\phi: \ \mathcal{A} \to \mathbb{C}^{n\times n}, \quad h \mapsto M_h.$$

M_h is the coordinate version of the filter h:

$$h(x)s(x) \bmod p(x) \Leftrightarrow M_h\mathbf{s}.$$

ϕ is a homomorphism (of algebras), i.e., $\phi(h(x)) = h(\phi(x))$ for all polynomials q.

In our example (5), the matrices $\phi(h)$ are precisely all circulant matrices. Thus, as well-known, circular convolution is equivalent to multiplying by a circulant matrix.

Shift matrix and visualization. Specifically, we call $\phi(x)$ the *shift matrix*. The graph that has $\phi(x)$ as adjacency matrix is called the *visualization* of the model (4). It visualizes the operation of the shift on the basis and, in a sense, the structure imposed on a vector **s** by the signal model. The signal values are associated with the nodes of the graph.

In our example (5), $\phi(x)$ is the circular shift matrix because $x \cdot x^\ell = x^{\ell+1} \bmod (x^n - 1)$. The associated graph is the circle shown in Fig. 3. The graph, as its infinite counterpart in Fig. 2, is *directed*. For this reason, we call (5) a finite *time model* [4].

Note that $p(x) = x^n - 1 = 0$ or $x^n = 1$ encodes the cyclic boundary condition. Reducing all x^k, $k \in \mathbb{Z}$, modulo $x^n - 1$ yields the periodic signal extension associated with this model.

Spectrum and Fourier transform. The spectral decomposition of the signal space $\mathcal{M}$ in the model (4) is given by the Chinese remainder theorem (CRT). It decomposes $\mathcal{M}$ into a

direct sum of one-dimensional $\mathcal{A}$-modules, the spectrum of $\mathcal{M}$:

$$\begin{aligned}\Delta:\ \mathbb{C}[x]/p(x) &\to \mathbb{C}[x]/(x-\alpha_0)\oplus\ldots\oplus\mathbb{C}[x]/(x-\alpha_{n-1}),\\ s=s(x)&\mapsto (s(\alpha_0),\ldots,s(\alpha_{n-1})).\end{aligned}$$

Δ is the Fourier transform for the model (4) and $\Delta(s)$ is the spectrum of the signal s.

With respect to the basis b of $\mathcal{M}$ and the bases $(x^0)=(1)$ in each of the $\mathbb{C}[x]/(x-\alpha_k)$, Δ is represented by a matrix, the so-called *polynomial transform*

$$\mathcal{P}_{b,\alpha}=[p_\ell(\alpha_k)]_{0\le k,\ell<n}.$$

As Δ, we also call $\mathcal{P}_{b,\alpha}$ a Fourier transform for the model (4). The algebraic theory establishes that the transform is invertible (with the above assumptions).

Computing the Fourier transform for a signal s becomes in coordinates the matrix-vector multiplication

$$\Delta(s)\Leftrightarrow \mathcal{P}_{b,\alpha}\mathbf{s}.$$

Choosing different bases (β_k) in the spectrum yields the *scaled* polynomial transform

$$\mathrm{diag}(1/\beta_0,\ldots,1/\beta_{n-1})\mathcal{P}_{b,\alpha}.$$

We call any polynomial transform (scaled or not) a Fourier transform for the model (4) and denote it with $\mathcal{F}$.

In our example (5), the zeros of x^n-1 are given by $\alpha=(\omega_n^0,\ldots,\omega_n^{n-1})$, $\omega_n=\exp(-2\pi j/n)$. Thus, the spectral decomposition is

$$\begin{aligned}\Delta:\ \mathbb{C}[x]/p(x) &\to \mathbb{C}[x]/(x-\omega_n^0)\oplus\ldots\oplus\mathbb{C}[x]/(x-\omega_n^{n-1}),\\ s=s(x)&\mapsto (s(\omega_n^0),\ldots,s(\omega_n^{n-1})).\end{aligned}$$

The polynomial transform is precisely the DFT:

$$\mathcal{P}_{b,\alpha}=[\omega_n^{k\ell}]_{0\le k,\ell<n}=\mathrm{DFT}_n\,.$$

This further motivates the notions of finite z-transform and finite time model introduced before.

Diagonalization properties. The algebraic theory asserts that the matrices diagonalized by any Fourier transform $\mathcal{F}$, i.e., (scaled) polynomial transform, are precisely the matrices $\phi(h)$, $h\in\mathcal{A}$. Specifically,

$$\mathcal{F}\phi(h)\mathcal{F}^{-1}=\mathrm{diag}(h(\alpha_0),\ldots,h(\alpha_{n-1})).$$

The collection of the $h(\alpha_k)$ is the *frequency response* of the filter h.

Applied to our example, this establishes that the DFT diagonalizes all circulant matrices, a well-known fact.

C. Finite Shift-Invariant Signal Models in 2-D

Extending the theory of the previous section to 2-D signal models is in most parts straightforward. The main difference is that in 2-D two shifts are available, which means we have to work with polynomial algebras in two variables x,y. Consequently, we now also need to compute modulo (at least) two polynomials $p(x,y),q(x,y)$ to make the polynomial algebras finite-dimensional.

Polynomial algebras (two variables). Let $p(x,y)$, $q(x,y)\in\mathbb{C}[x,y]$ be two polynomials in two variables. For simplicity, we require that both polynomials have the same total degree[4] n and that the leading term, i.e., the term of highest degree, of $p(x,y)$ is x^n and the leading term of $q(x,y)$ is y^n. The polynomial algebra in two variables corresponding to $p(x,y)$ and $q(x,y)$ is written as

$$\mathcal{A}=\mathbb{C}[x,y]/\langle p(x,y),q(x,y)\rangle.$$

As in the univariate case $\mathcal{A}$ is a vector space, but also an algebra if we define multiplication modulo $p(x,y)$ and $q(x,y)$. This is done by performing division with remainder as far as possible with respect to $p(x,y)$ and $q(x,y)$.[5]

The dimension of $\mathcal{A}$ is n^2; a possible choice of basis for $\mathcal{A}$ is $\{x^iy^j\mid i,j=0,\ldots,n-1\}$. We require in addition that the set $\alpha=\{(\mu,\nu)\in\mathbb{C}^2\mid p(\mu,\nu)=q(\mu,\nu)=0\}$ of common zeros has the maximum possible cardinality n^2.

Signal model built from polynomial algebras. We set $\mathcal{A}=\mathcal{M}=\mathbb{C}[x,y]/\langle p(x,y),q(x,y)\rangle$. Let $b=(p_0,\ldots,p_{n^2-1})$ be a basis of $\mathcal{M}$. Then we can define a signal model through

$$\Phi:\mathbb{C}^{n^2}\to\mathcal{M},\ \mathbf{s}\mapsto s=s(x,y)=\sum_{0\le\ell<n^2}s_\ell p_\ell(x,y). \quad (6)$$

Filter and signals both are polynomials in two variables, $h=h(x,y)$, $s=s(x,y)$. Filtering is the multiplication hs modulo p and q.

Filtering in coordinates. Every filter $h=h(x,y)$ is a linear mapping, and thus can be represented by a matrix M_h with respect to the basis b. This defines a mapping

$$\phi:\ \mathcal{A}\to\mathbb{C}^{n^2\times n^2},\quad h\mapsto M_h,$$

i.e., M_h is the coordinate version of the filter with respect to the basis b. Filtering in coordinates thus becomes

$$h(x,y)s(x,y)\bmod\langle p(x,y),q(x,y)\rangle\Leftrightarrow M_h\mathbf{s}.$$

ϕ is a homomorphism (of algebras), i.e., $\phi(h(x,y))=h(\phi(x),\phi(y))$ for all polynomials h.

Shift matrices and visualization. In difference to the 1-D case, we now have two shift matrices, namely $\phi(x)$ and $\phi(y)$, i.e., two associated graphs with the same set of nodes. We visualize the model (6) by superimposing these graphs, i.e., by the graph that has $\phi(x)+\phi(y)$ as adjacency matrix.

Spectrum and Fourier transform. In the 2-D case the CRT again gives the spectral decomposition of the signal space $\mathcal{M}$ in the model (6). By assumption the polynomials $p(x,y)$ and $q(x,y)$ have n^2 distinct common zeros $\alpha=((\mu_0,\nu_0),\ldots,(\mu_{n^2-1},\nu_{n^2-1}))$. Now, the CRT decomposes $\mathcal{M}=\mathbb{C}[x,y]/\langle p(x,y),q(x,y)\rangle$ into a direct sum of n^2 one-dimensional $\mathcal{A}$-modules, the spectrum of $\mathcal{M}$:

$$\begin{aligned}\Delta:\ \mathcal{M}\ &\to\textstyle\bigoplus_{0\le i<n^2}\mathbb{C}[x,y]/\langle x-\mu_i,y-\nu_i\rangle,\\ s=s(x,y)&\mapsto(s(\mu_0,\nu_0),\ldots,s(\mu_{n^2-1},\nu_{n^2-1})).\end{aligned} \quad (7)$$

[4]The total degree of $p(x,y)$ is the largest $a+b$ over all summands cx^ay^b of p.

[5]Strictly speaking the algebra is defined by computing modulo the *ideal* generated by $p(x,y)$ and $q(x,y)$, see [18]. In general, an ideal may have more than two generators, but not in this paper. Also, the simple greedy algorithm of performing division with remainder with respect to $p(x,y)$ and $q(x,y)$ works in our situation; in general a Gröbner basis is required [18].

Δ is the Fourier transform for the model (6) and $\Delta(s)$ is the spectrum of the signal s. Choosing the basis b in $\mathcal{M}$ and (1) in each spectral component, Δ is represented by the matrix

$$\mathcal{P}_{b,\alpha} = [p_\ell(\mu_k, \nu_k)]_{0 \le k,\ell < n^2},$$

which we call a 2-D polynomial transform and also a Fourier transform. Invertibility is guaranteed under by the algebraic theory under the above assumptions.

As in the 1-D case choosing different bases in the spectrum yields a *scaled* polynomial transform $\mathcal{F}$.

Diagonalization properties. The Fourier transform $\mathcal{F}$ diagonalizes precisely the matrices $\phi(h)$, where $h = h(x, y) \in \mathcal{A}$. Specifically,

$$\mathcal{F}\phi(h)\mathcal{F}^{-1} = \mathrm{diag}(h(\mu_0, \nu_0), \ldots, h(\mu_{n^2-1}, \nu_{n^2-1})).$$

The collection of the $h(\mu_k, \nu_k)$ is the frequency response of the filter h.

The separable case. There is a simple way to construct a 2-D signal model from a 1-D signal model $(\mathcal{A}, \mathcal{M}, \Phi)$ as explained in [5]. Consider the 1-D signal model for $\mathbb{C}^n$ in (4), which implicitly fixes the basis $b = (p_0, \ldots, p_{n-1})$ and $\mathcal{A} = \mathcal{M} = \mathbb{C}[x]/p(x)$.

The corresponding *separable* 2-D model is obtained by setting

$$\begin{aligned} \mathcal{A} \times \mathcal{A} &= \mathcal{M} \times \mathcal{M} = \mathbb{C}[x]/p(x) \otimes \mathbb{C}[y]/p(y) \\ &= \mathbb{C}[x, y]/\langle p(x), p(y) \rangle \end{aligned}$$

and

$$\begin{aligned} \Phi \quad : \quad & \mathbb{C}^{n \times n} \to \mathcal{M} \times \mathcal{M}, \\ & \mathbf{s} \mapsto s = s(x, y) = \sum_{0 \le k,\ell < n} s_{k,\ell} p_k(x) p_\ell(y). \end{aligned}$$

The model is usually adopted for a square $n \times n$ array of signal values $\mathbf{s} \in \mathbb{C}^{n \times n}$; we emphasize this by writing $\mathbb{C}^{n \times n}$ instead of $\mathbb{C}^{n^2}$.

A Fourier transform for this model is simply the Kronecker product of $\mathcal{P}_{b,\alpha}$ with itself. The visualization of the model is the direct product of the 1-D visualization (the graph) with itself. The adjacency matrix of this graph is $\phi(x) \otimes \mathrm{I}_n + \mathrm{I}_n \otimes \phi(y)$. Examples are shown in Figs. 1(a) and (b) (without the boundary conditions).

The signal models derived in this paper are nonseparable.

III. Infinite 1-D Space Models

So far, we have introduced the general framework (provided by the algebraic theory of signal processing) for shift-invariant signal processing, focusing on the finite case. This framework will also provide the underpinning for the spatial hexagonal lattice. However, the question is how to derive the appropriate signal model to apply the theory.

In [4] we introduced a procedure for deriving signal models from basic principles and used it to derive the well-known infinite and finite time models discussed before, but also to derive infinite and finite *space* models. Space, in the algebraic theory, means that the model is undirected versus the directed signal models associated with time. This will become clearer below.

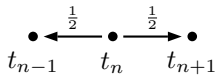

Fig. 4. The space shift $q \diamond t_n$.

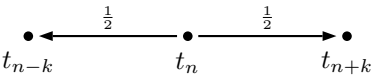

Fig. 5. The k-fold space shift $q_k \diamond t_n$.

We introduce the procedure in this section by sketching the derivation of 1-D space models, which eventually leads to the DCTs and DSTs as associated Fourier transforms. The same derivation will later yield the signal models for the spatial hexagonal lattice and also highlight the analogy between 1-D DCTs and the new transforms to be introduced later.

The detailed version of the derivation can be found in [5], which also contains all the proofs.

A. Derivation

The derivation of the discrete 1-D space model (as the derivation of the other 1-D models in [3]) follows three steps: definition of the shift, linear extension, and realization.

Definition of the shift. To define a suitable shift operator q, we first need a set of *space marks* $(t_n)_{n \in \mathbb{Z}}$, the shift can operate on. These marks will later be associated with the discrete signal values. We denote the shift operation abstractly with $\diamond$. The well-known time shift would be defined as $q \diamond t_n = t_{n+1}$; the below derivation would yield the z-transform and DTFT in the infinite case, and the finite z-transform and DFT in the finite case.

Since we want an undirected model, the shift has to operate symmetrically. The simplest choice is

$$q \diamond t_n = \frac{1}{2}(t_{n-1} + t_{n+1}), \tag{8}$$

which we call the (1-D) space shift. It is visualized in Fig. 4.

Next, we need a k-fold space shift q_k. A suitable definition is

$$q_k \diamond t_n = \frac{1}{2}(t_{n-k} + t_{n+k}). \tag{9}$$

It is visualized in Fig. 5. Every space mark is reachable from t_n with exactly one k-fold space shift, $k \ge 0$.

From the definition it follows that $q_k = T_k(q)$ is the Chebyshev polynomial of the first kind and degree k. This becomes clear from the power form of T_k; see Table III in Appendix A, which we invite the reader to read at this point.

Linear extension. We first linearly extend the operation of q to the entire vector space $\mathcal{M} = \{\sum_{n \in \mathbb{Z}} s_n t_n\}$ and then to the operator domain $\mathcal{A} = \{\sum_{k \ge 0} h_k T_k(q)\}$. $\mathcal{M}$ will become our signal module, and $\mathcal{A}$ the associated filter algebra. Note that $\mathcal{A}$ contains only right-sided sequences since $T_{-k} = T_k$ (because this holds for q_k in (9)).

Through the linear extension, filtering for $s \in \mathcal{M}$ and $h \in \mathcal{A}$ is now abstractly defined as

$$\sum_{k \ge 0} h_k T_k(q) \diamond \sum_{n \in \mathbb{Z}} s_n t_n = \sum_{n \in \mathbb{Z}} \sum_{i+j=n} h_i s_j (T_i(q) \diamond t_j). \tag{10}$$

Since the sums are infinite we have to take care of convergence issues. This will be done next as part of the realization.

Realization. The realization replaces the abstract shift and space marks with concrete objects. We do this by setting $q = x$ and $\diamond = \cdot$ (the ordinary multiplication). The space marks are now determined as polynomials of x. Namely, (8) is now equivalent to

$$t_{n+1} = 2xt_n - t_{n-1},$$

which is precisely the recursion for the general Chebyshev polynomials (see (35) in Appendix A). Thus,

$$t_n = C_n(x).$$

After normalizing $C_0 = 1$, there is a degree of freedom in how to choose C_1 as a polynomial of degree 1; C_0 and C_1 together then determine all C_n, $n \in \mathbb{Z}$. Since $\deg(C_n) = n$ for $n \geq 0$, $\{C_n \mid n \geq 0\}$ is a basis of all polynomials $\mathbb{C}[x]$. Since every C_{-m}, $m > 0$ is also a polynomial of degree at most m, it can be written as

$$C_{-m} = \sum_{0 \leq \ell \leq m} s_\ell C_\ell, \tag{11}$$

where $s_\ell \in \mathbb{C}$. In other words, the left half of the sequence $n < 0$ depends on the right half $n \geq 0$. As a consequence, $\mathcal{M}$ can contain only right-sided sequences $\sum_{n \geq 0} s_n C_n$ and (11) encodes the left signal extension associated with $\mathcal{M}$.

Since we have a degree of freedom in choosing C_1, we force the simplest possible signal extension, called *monomial* signal extension. This means that in (11), the sum has at most one summand for all $m > 0$. As shown in [5], there are exactly four series of Chebyshev polynomials that yield a monomial signal extension, denoted with $C = T, U, V, W$. They are called, respectively, the Chebyshev polynomials of the first, second, third, and fourth kind; the first two kinds are explained in Appendix A. For $C = T$, (11) becomes $T_{-m} = T_m$, i.e., the signal extension is whole-point symmetric; for $C = U$, $U_{-m} = -U_{m-2}$ holds, which is whole-point antisymmetric and implies $U_{-1} = 0$.

Filtering as in (10) (for right-sided signals) converges if $\mathbf{h} \in \ell^1(\mathbb{N})$ and $\mathbf{s} \in \ell^2(\mathbb{N})$.

Infinite 1-D space models. In summary, we obtained four infinite space signal models $(\mathcal{A}, \mathcal{M}, \Phi)$ for $V = \ell^2(\mathbb{N})$, collectively described by

$$\begin{aligned} \mathcal{A} &= \{h = \textstyle\sum_{k \geq 0} h_k T_k(x) \mid \mathbf{h} \in \ell^1(\mathbb{N})\}, \\ \mathcal{M} &= \{s = \textstyle\sum_{n \geq 0} s_n C_n(x) \mid \mathbf{s} \in \ell^2(\mathbb{N})\}, \\ \Phi &: \ V \to \mathcal{M}, \ \mathbf{s} \mapsto \textstyle\sum_{n \geq 0} s_n C_n(x), \end{aligned} \tag{12}$$

where $C \in \{T, U, V, W\}$. Φ is called the C-transform, or if the choice is specified, T-, U-, V-, W-transform. Note that the filters are represented as series in the k-fold space shifts T_k, independent of the choice of C. Filtering in this model is the multiplication hs, where $h \in \mathcal{A}$ and $s \in \mathcal{M}$. The corresponding operation on the coordinate vectors $\mathbf{h}$ and $\mathbf{s}$ (not shown here) is the associated notion of convolution.

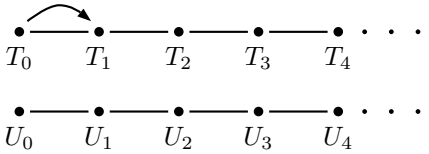

Fig. 6. Visualization of the infinite space models given by the C-transform for $C \in \{T, U\}$. For each internal edge, the arrows go in both directions and are thus omitted. Also, the common edge scaling factor $1/2$ is omitted.

B. Properties

Visualization. The visualization of the above models are obtained by letting the shift x operate on the basis. For the T- and U-transform we obtain the two graphs in Fig. 6 (the common factor of $1/2$ is omitted). Note that the graphs are undirected, which motivates the notion of space model.

For the T-transform, the extra arrow from T_0 to T_1 represents the left b.c. $T_{-1} = T_1$. Similarly, for the U-transform $U_{-1} = 0$ implies the absence of this arrow.

Spectrum and Fourier transform. The infinite space models in (12) have an associated notion of spectrum, Fourier transform, and frequency response [5]. We will not show them here due to space limitations and to focus on the finite case discussed next.

IV. Derivation of Finite 1-D Space Models

To obtain finite space models associated with the infinite ones in (12) is only a small step. Since these models should also be shift-invariant we know already that their underlying structure will be provided by polynomial algebras. The question is how to construct them. In particular, the crucial question is how to choose $p(x)$ in (4), which determines the filter algebra and the signal module, the notion of filtering, and the spectrum. It turns out that the choice of $p(x)$ is equivalent to the design of proper boundary conditions.

A. Derivation

We want to build a model for discrete finite signals $\mathbf{s} = (s_0, \ldots, s_{n-1}) \in \mathbb{C}^n$. Following the same steps as in the finite case seems to lead to a signal space consisting of polynomials of degree less than n represented as

$$s = s(x) = \sum_{0 \leq \ell < n} s_\ell C_\ell(x). \tag{13}$$

As discussed before, the choice of C determines the left boundary condition and the left signal extension. Four choices of C lead to a monomial extension. However, in the finite case we also have to take care of the right boundary.

Right boundary. The problem with (13) is that these polynomials are not closed under the shift operation, since multiplying by x increases the degree. Specifically,

$$xC_{n-1} = \frac{1}{2}(C_{n-2} + C_n)$$

has degree n. This can be fixed by introducing a *right b.c.* that expresses C_n as a linear combination of $C_0, \ldots, C_{n-1}$

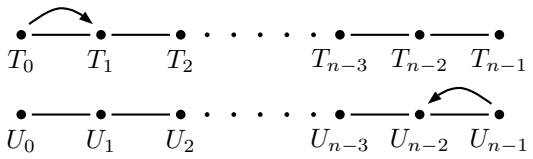

Fig. 7. Visualizations of the finite space models for which the DCT, type 3 (above) and the DST, type 3 (below) are Fourier transforms. Again, the common edge scaling factor $1/2$ is omitted.

and effectively reduces the degree again:

$$C_n = \sum_{0\le\ell<n} \beta_\ell C_\ell \quad \Leftrightarrow \quad p(x) = C_n - \sum_{0\le\ell<n} \beta_\ell C_\ell = 0.$$

Mathematically, this means that the signal space becomes the polynomial algebra $\mathcal{M} = \mathbb{C}[x]/p(x)$. So we get the desired structure and understand that the choice of p is equivalent to the right b.c., which in turn determines the entire right signal extension by reducing C_ℓ, $\ell \ge n$ modulo p.

Again, we are interested in the simplest, i.e., monomial signal extension. It turns out that for each of the four choices of C there are four possible right b.c., leading to a total of 16 finite space models corresponding to 16 DCTs/DSTs as associated Fourier transforms.

We consider two cases. For $C = T$, the b.c. $T_n = 0$ implies the right signal extension $T_{n+k} = -T_{n-k}$. For $C = U$, $2T_n = U_n - U_{n-2}$ implies the b.c. $U_n = U_{n-2}$ and the right signal extension $U_{n+k} = U_{n-k-2}$.

Finite 1-D space models. We only state the above two out of sixteen finite space models since they have corresponding 2-D hexagonal space models derived later.

The two signal models are simultaneously defined by

$$\mathcal{A} = \mathcal{M} = \mathbb{C}[x]/T_n, \quad \Phi: \ \mathbf{s} \mapsto \sum_{0\le\ell<n} s_\ell C_\ell, \qquad (14)$$

where $C \in \{T, U\}$. We call Φ a finite T-transform or U-transform.

In both cases, the elements of $\mathcal{A}$ (the filters) are expressed as $h = \sum_{0\le k<n} h_k T_k$, i.e., as combination of k-fold space shifts. Filtering in both cases is the multiplication of polynomials modulo T_n. The difference is in the choice of basis in $\mathcal{M}$.

B. Properties

Visualization. In (14) for $C = T$, the left b.c. is $s_{-1} = s_1$, since $C = T$. The right b.c. is $s_n = 0$, since $T_n = 0$ in $\mathcal{M}$. The operation of the shift yields the visualization in Fig. 7 (top).

In (14) for $C = U$, the b.c.'s are reversed. The U-basis in $\mathcal{M}$ asserts $s_{-1} = 0$, since $U_{-1} = 0$, and $U_n - U_{n-2} = 0$ implies $s_n = s_{n-2}$. The visualization is shown in Fig. 7 (bottom).

Fourier transform. We consider (14) for $C = T$. The zeros of T_n are given in Table III in Appendix A as $\alpha_k = \cos(k + 1/2)\pi/n$, $0 \le k < n$. The (polynomial) Fourier transform is thus given by the DCT, type 3:

$$\mathcal{F} = \mathcal{P}_{b,\alpha} = [T_\ell(\cos(k + 1/2)\pi/n)]_{0\le k,\ell<n} = \text{DCT-3}_n.$$

Similarly, (14) for $C = U$ has the DST, type 3 as associated Fourier transform (a scaled polynomial transform in this case).

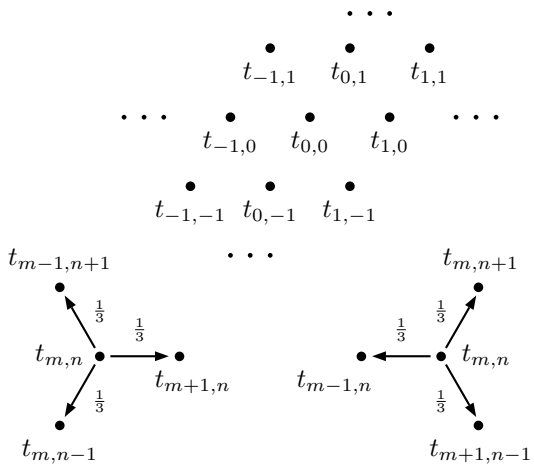

Fig. 8. A hexagonal array of space marks and two hexagonal space shifts $q \diamond t_{m,n}$ and $\overline{q} \diamond t_{m,n}$ operating on it.

Unitary version. The DCT-3$_n$ and DST-3$_n$ diagonalize the adjacency matrices of the two graphs (i.e., the shift matrices) in Fig. 7, respectively. Since these are almost symmetric (since the graphs are undirected except for the boundary), the transforms are almost unitary. Indeed, as it is well-known, suitable scaling factors make the transforms unitary and even orthogonal. Their derivation is explained, e.g., in [5].

Separable extension to 2-D. The separable extension of the 1-D space models to 2-D is straightforward using the theory in Section II-C. Fig. 1(b) visualizes the models obtained (without boundary conditions).

V. Infinite 2-D Hexagonal Space Model

A. Derivation

The derivation of a signal model for the 2-D hexagonal spatial lattice is completely analogous to the derivation of the 1-D space models in Section III-A. The reader may want to frequently go back to that section to get a better intuition for the proceedings here. The crucial starting point for the derivation of the hexagonal space model is the proper choice of two shifts.

Definition of the shifts. First, we define a 2-D array of space marks $(t_{m,n})_{m,n\in\mathbb{Z}}$, assumed to be arranged on a *hexagonal*[6] lattice as shown in Fig. 8 (left). Since we derive a 2-D model, we need two shift operators $q, \overline{q}$. Every space mark has six neighbors, so each shift should contain three. A proper definition is

$$q \diamond t_{m,n} = \frac{1}{3}(t_{m+1,n} + t_{m,n-1} + t_{m-1,n+1}), \qquad (15)$$

$$\overline{q} \diamond t_{m,n} = \frac{1}{3}(t_{m,n+1} + t_{m-1,n} + t_{m+1,n-1}). \qquad (16)$$

They are visualized in Fig. 8 (right). Overlaying these shifts on the hexagonal lattice yields each edge in each direction. This will later make the model undirected, i.e., spatial, as desired.

[6]Every point has at equal distance six neighbors, which form a hexagon.

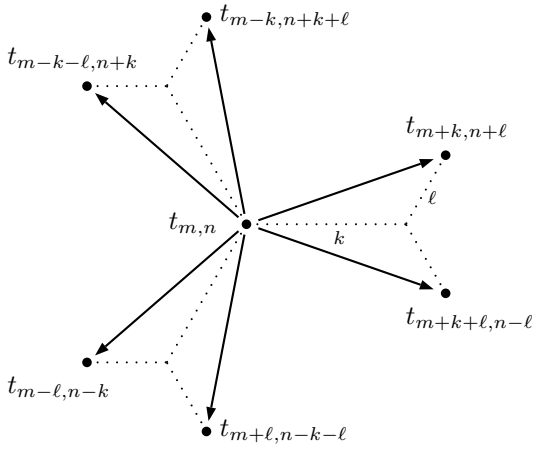

Fig. 9. The (k,ℓ)-fold hexagonal space shift $q_{k,\ell}$; the common edge weight of $1/6$ is omitted. In particular, $q_{1,0} = q,\ q_{0,1} = \overline{q}$.

Next, we need a (k,ℓ)-fold shift $q_{k,\ell}$. The proper definition is

$$q_{k,\ell} \diamond t_{m,n} = \frac{1}{6}(t_{m+k,n+\ell} + t_{m+k+\ell,n-\ell} + t_{m+\ell,n-k-\ell} + t_{m-\ell,n-k} + t_{m-k-\ell,n+k} + t_{m-k,n+k+\ell}) \quad (17)$$

and is visualized in Fig. 9. In particular,

$$q_{k,0} \diamond t_{m,n} = \frac{1}{3}(t_{m+k,n} + t_{m,n-k} + t_{m-k,n+k}), \quad (18)$$

$$q_{0,\ell} \diamond t_{m,n} = \frac{1}{3}(t_{m,n+\ell} + t_{m-\ell,n} + t_{m+\ell,n-\ell}). \quad (19)$$

Note that for any space mark $t_{m,n}$ every point in the hexagonal lattice is reachable with exactly one (k,ℓ)-fold shift, $k,\ell \geq 0$. Further, $q = q_{1,0}$ and $\overline{q} = q_{0,1}$.

Here, the Chebyshev polynomials in two variables (of the first kind) come into play the first time. We invite the reader to read Appendix B at this point.

Lemma 1 The (k,ℓ)-fold shift is a polynomial in $q, \overline{q}$. Specifically,

$$q_{k,\ell} = T_{k,\ell}(q, \overline{q}),$$

where $T_{k,\ell}$ denotes the Chebyshev polynomial of the first kind in two variables.

Proof: The assertion follows from the power form on $T_{k,\ell}$ shown in Table IV in Appendix B. ■

Linear extension. As in the 1-D case, we extend the shift operation $\diamond$ linearly first to the entire vector space $\mathcal{M} = \{\sum_{m,n\in\mathbb{Z}} s_{m,n} t_{m,n}\}$ and then to the operator domain $\mathcal{A} = \{\sum_{k,\ell\geq 0} h_{k,\ell} T_{k,\ell}(q,\overline{q})\}$; k,ℓ are non-negative, since the symmetry properties of $T_{k,\ell}$ (see Appendix B) show that each $T_{k,\ell}$ is equal to a $T_{k',\ell'}$ with $k',\ell' \geq 0$. Specifically, for $k,\ell \geq 0$, $T_{-k,-\ell} = T_{\ell,k}$, and

$$T_{-k,\ell} = \begin{cases} T_{k,\ell-k} & \ell \geq k \\ T_{\ell,k-\ell} & \ell < k \end{cases},\ T_{k,-\ell} = \begin{cases} T_{k-\ell,\ell} & k \geq \ell \\ T_{\ell-k,k} & k < \ell \end{cases}. \quad (20)$$

$\mathcal{M}$ will become the signal space and $\mathcal{A}$ the associated algebra of filters. Filtering is defined through the linear extension of $\diamond$ to $\mathcal{A}$ and $\mathcal{M}$:

$$\sum_{k,\ell\geq 0} h_{k,\ell} T_{k,\ell}(q,\overline{q}) \diamond \sum_{m,n\in\mathbb{Z}} s_{m,n} t_{m,n} = \sum_{m,n\in\mathbb{Z}} \sum_{i+j=m,k+\ell=n} h_{i,k} s_{j,\ell} (T_{i,k}(q,\overline{q}) \diamond t_{j,\ell}). \quad (21)$$

Convergence issues and boundaries will be handled next.

Realization. For the realization, we set $q = x, \overline{q} = y$, and $\diamond = \cdot$ (multiplication). The space marks $t_{m,n}$ are now determined as polynomials in two variables. Namely, (15) and (16) are precisely equivalent to the two recurrences for the general Chebyshev polynomials in two variables (see (40) and (41) in Appendix B). Thus,

$$t_{m,n} = C_{m,n}(x,y).$$

Appendix A asserts that six initial conditions are needed to determine the entire array $(C_{m,n} \mid m,n \in \mathbb{Z})$, namely $C_{0,0} = 1, C_{0,1}, C_{0,2}, C_{1,0}, C_{1,1}, C_{2,0}$. As in the 1-D case, the question is which choices yield a simple, ideally monomial signal extension? In the 1-D case we proved that there are exactly four choices [5]. Here, the situation is more complicated: we do not have an exhaustive characterization, but give only two choices of $C_{m,n}$, which provide a monomial extension. Namely, as one may expect, the Chebyshev polynomials of the first and second kind in two variables (see Appendix B): T and U. The monomial extension in both cases follows from the symmetry properties in Table IV, Appendix B.

For $C = T$, that table establishes symmetry with respect to both x-axis (formed by all space marks $t_{k,0}$) and y-axis (formed by all space marks $t_{0,\ell}$) in the hexagonal lattice. Using this symmetry, every $T_{m,n}$ with $m < 0$ or $n < 0$ is a $T_{m',n'}$ with $m', n' > 0$ as already explained in (20). In particular, we have the left and bottom boundary conditions

$$T_{-1,\ell} = T_{1,\ell-1} \quad \text{(left boundary)}, \quad (22)$$

$$T_{k,-1} = T_{k-1,1} \quad \text{(bottom boundary)}. \quad (23)$$

Similarly, for $C = U$, Table IV establishes antisymmetry with respect to the two axes given by the space marks $t_{k,-1}$ and $t_{-1,\ell}$, respectively. The left and bottom boundary is thus given by $U_{-1,\ell} = U_{k,-1} = 0$.

This discussion establishes that the hexagonal space model will be for 2-D signals on the positive quadrant $\mathbb{N} \times \mathbb{N}$ only. Convergence of filtering as in (21) for these signals is guaranteed if $\mathbf{h} \in \ell^1(\mathbb{N}\times\mathbb{N})$ and $\mathbf{s} \in \ell^2(\mathbb{N}\times\mathbb{N})$.

Infinite 2-D hexagonal space models. In summary, we obtain two infinite hexagonal space models $(\mathcal{A}, \mathcal{M}, \Phi)$ for $V = \ell^2(\mathbb{N}\times\mathbb{N})$. They are jointly defined by

$$\begin{aligned} &\mathcal{A} = \{h = \textstyle\sum_{k,\ell\geq 0} h_{k,\ell} T_{k,\ell}(x,y) \mid \mathbf{h} \in \ell^1(\mathbb{N}\times\mathbb{N})\}, \\ &\mathcal{M} = \{s = \textstyle\sum_{m,n\geq 0} s_{m,n} C_{m,n}(x) \mid \mathbf{s} \in \ell^2(\mathbb{N}\times\mathbb{N})\}, \\ &\Phi:\ V \to \mathcal{M},\ \mathbf{s} \mapsto \textstyle\sum_{m,n\geq 0} s_{m,n} C_{m,n}(x,y), \end{aligned} \quad (24)$$

where $C \in \{T, U\}$. We call Φ the 2-D hexagonal C-transform or, if specified, T- or U-transform. Note that independent of C, the filters are represented as series in $T_{k,\ell}$, the (k,ℓ)-fold space shifts.

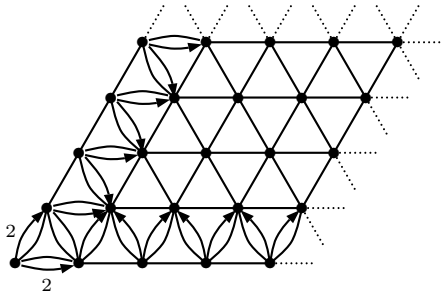

(a) Visualization for $C = T$

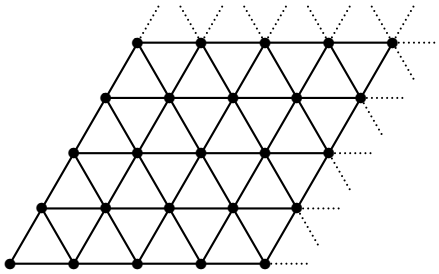

(b) Visualization for $C = U$

Fig. 10. Visualizations of the two infinite spatial hexagonal signal models given in (24): (a) 2-D hexagonal T-transform; and (b) 2-D hexagonal U-transform. The common edge weight factor of $1/3$ is omitted.

Filtering in this model is the multiplication hs of series $h \in \mathcal{A}$, $s \in \mathcal{M}$, and can be evaluated using (21) and (17). The corresponding operation on the coordinate sequences **h** and **s** is the associated notion of convolution.

B. Properties

Visualization. In (24) we have to distinguish the cases $C = T$ and $C = U$. If $C = T$ then the left and bottom b.c.'s are given by (22) and (23). The operation of the two shifts yields the visualization in Fig. 10(a).

Due to the antisymmetry with respect to the coordinate axes we get $U_{k,-1} = U_{-1,\ell} = 0$ for all $k, \ell \in \mathbb{Z}$. Thus, the operation of the two shifts yields the visualization in Fig. 10(b).

Spectrum and Fourier transform. The spectrum and Fourier transform for the models (24) are obtained similarly as for the infinite 1-D space models [5], namely by expanding $s = \sum s_{m,n} C_{m,n}(x, y)$ using the power form of C and setting $u = e^{j\omega_1}$ and $v = e^{j\omega_2}$. The frequency response of a filter h is obtained in the same way. The spectrum is periodic in ω_1 and ω_2 but has additional six-fold symmetry, which reduces the domain to the triangle in Fig. 11(c) with symmetric b.c.'s. For contrast, Fig. 11(a) and (b) visualize the spectrum of the 2-D z-transform (periodic in both dimensions) and the 2-D T-transform (symmetric in both dimensions on the smaller domain shown, since the spectrum possesses a four-fold symmetry).

In other words, in Fig. 11(b) the torus (square with periodic b.c.'s) in Fig. 11 is partitioned into four squares as shown. In Fig. 11(c) the torus is partitioned into six triangles as shown. Note that four of these triangles cross the boundary of the large square in the representation, which is displayed dashed for this reason.

Fig. 11(c) was obtained by slightly adapting [19], which studies the dual situation to this paper, namely, in SP terms, 2-D continuous signals that are defined on a triangle and symmetrically extended to the entire plane.

VI. Finite Hexagonal Space Model

The derivation of the finite hexagonal space model is analogous to the derivation of the 1-D space model in Section IV. This means, the problem is in designing the boundary conditions and thus the proper polynomial algebra. The general theory in Section II-C then provides all basic SP concepts and in particular, the associated Fourier transform.

A. Derivation

We build a model for an $n \times n$ array of signal values $(s_{k,\ell})_{0 \le k,\ell < n} \in \mathbb{C}^{n \times n}$.[7] Following the derivation steps in Section V leads to a signal space consisting of polynomials in two variables, represented as

$$s = s(x, y) = \sum_{0 \le k,\ell < n} s_{k,\ell} C_{k,\ell}(x, y), \tag{25}$$

where $C = T$ or $C = U$ to ensure a monomial left and bottom signal extension. Since the array is now finite, we also have to take care of the right ($k \ge n$) and upper ($\ell \ge n$) boundary.

Right and upper boundary. Applying an x- or y-shift to a space mark $C_{n-1,\ell}$ at the right boundary or a space mark $C_{k,n-1}$ at the upper boundary leaves the array. For example,

$$xC_{n-1,\ell} = \frac{1}{3}(C_{n,\ell} + C_{n-1,\ell-1} + C_{n-2,\ell+1});$$

$C_{n,\ell}$ is outside the array. In other words, the set of polynomials in (25) is not closed under shifting. To remedy this problem, we introduce right and upper boundary conditions, which in turn define right and upper signal extensions. Again, we aim for the simplest signal extension. However, in this case a monomial signal extension seems to be not achievable, only a 2-monomial extension. This means that every $C_{u,v}$ with $u \ge n$ or $v \ge n$ is a linear combination of at most two $C_{k,\ell}$ inside the array.

Due to the more complicated structure of the model, unlike in the 1-D case, we do not claim an exhaustive list of reasonable possible signal extensions. Rather, we provide for each of the two infinite models in (24) one choice, thus obtaining two finite models.

We consider $C = T$ and claim that

$$\mathcal{A} = \mathcal{M} = \mathbb{C}[x, y]/\langle T_{n,0}, T_{0,n} \rangle \tag{26}$$

yields the desired extension. First, we compute the right and upper boundary. $T_{n,0} = 0$ implies that

$$\begin{aligned} 0 &= T_{0,k} T_{n,0} = \frac{1}{3}(T_{n,k} + T_{n-k,0} + T_{n+k,-k}) \\ &= \frac{2}{3} T_{n,k} + \frac{1}{3} T_{n-k,0}, \end{aligned}$$

[7] Extending the discussion to $m \times n$ arrays is straightforward.

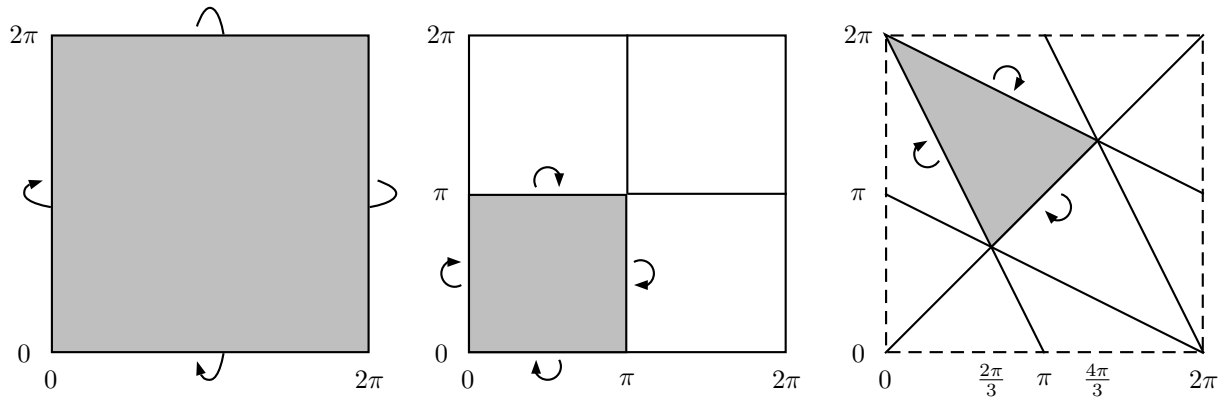

(a) 2-D z-transform (b) 2-D T-transform (c) 2-D hexagonal T-transform

Fig. 11. Visualization of the spectral domains (gray area) of the infinite 2-D time, space, and hexagonal space models in the ω_1, ω_2 plane. The symmetries, or boundary conditions, are apparent through (x, y) parameterizations: (a) $(e^{j\omega_1}, e^{j\omega_2})$ (periodic); (b) $(\cos(\omega_1), \cos(\omega_2))$ (symmetric); (c) $\frac{1}{3}(e^{j\omega_1} + e^{j\omega_2} + e^{-j(\omega_1+\omega_2)}, e^{-j\omega_1} + e^{-j\omega_2} + e^{j(\omega_1+\omega_2)})$ (symmetric). The U-transforms' parameterizations yield antisymmetric b.c.'s in (b) and (c).

where we used (18) and (20). The same computation can be performed starting with $T_{0,n} = 0$. We get

$$T_{n,\ell} = -\frac{1}{2} T_{n-\ell,0} \quad \text{(right boundary)}, \tag{27}$$

$$T_{k,n} = -\frac{1}{2} T_{0,n-k} \quad \text{(upper boundary)}. \tag{28}$$

The left and bottom boundaries are the same as in the infinite model (22) and (23).

To get the right signal extension, we multiply (27) by $T_{k,0}$ using again (18) and use the symmetry properties in (20). Similarly, we multiply (28) by $T_{0,\ell}$ to get the upper signal extension. The result is

$$T_{n+k,\ell} = -T_{n-k,\ell+k} - T_{n-k-\ell,k},$$
$$T_{k,n+\ell} = -T_{k+\ell,n-\ell} - T_{\ell,n-k-\ell}.$$

For $C = U$, we use the same algebra and module (26) as in the previous case. The effect is a different set of boundary conditions and signal extension obtained analogous to above. Namely, $T_{n,0} = 0$ implies $U_{n,0} = U_{n-2,1} - U_{n-3,0}$ (using (43) in Appendix B). Multiplying this equation with $T_{0,\ell}$ yields the right boundary $U_{n,\ell}$. The upper boundary is obtained similarly, starting with $T_{0,n} = 0$. The result is

$$U_{n,\ell} = U_{n-2,\ell+1} - U_{n-3-\ell,0} \quad \text{(right boundary)}, \tag{29}$$

$$U_{k,n} = U_{k+1,n-2} - U_{0,n-3-k} \quad \text{(upper boundary)}. \tag{30}$$

Finite 2-D hexagonal space models. We derived two finite signal models for $V = \mathbb{C}^{n \times n}$. They are jointly defined by

$$\begin{aligned} &\mathcal{A} = \mathcal{M} = \mathbb{C}[x, y]/\langle T_{n,0}, T_{0,n} \rangle, \\ &\Phi : \ \mathbf{s} \mapsto \textstyle\sum_{0 \le k,\ell < n} s_{k,\ell} C_{k,\ell}, \end{aligned} \tag{31}$$

where $C = T$ or $C = U$. We call Φ the finite 2-D hexagonal C-transform (or T- or U-transform). Both models are regular. The basis in $\mathcal{A}$ consists, independent of C, of the (k, ℓ)-fold space shifts $T_{k,\ell}$.

Filtering in this model is the multiplication hs of polynomials $h \in \mathcal{A}$ and $s \in \mathcal{M}$ modulo $T_{n,0}$ and $T_{0,n}$. It can be computed using (17) and (27) and (28) for the modulo reduction. The effect on the coordinate sequences **h** and **s** is the associated notion of convolution.

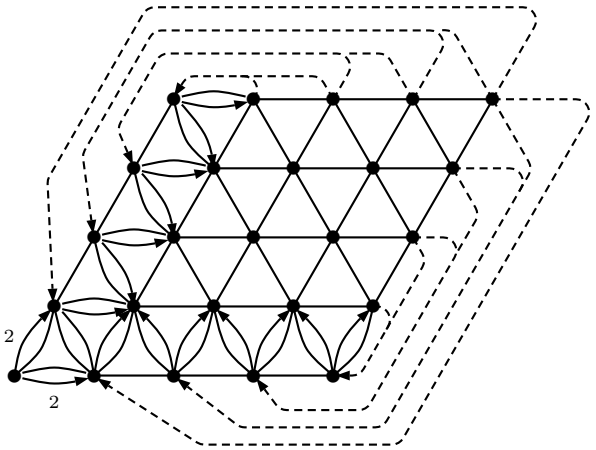

Fig. 12. Visualization of the finite 2-D hexagonal space model for which the DTT, type 1, is a Fourier transform (the case $n = 5$ is shown). For all solid (dashed) lines a common edge scaling factor of $1/3$ ($-1/2$) is omitted.

B. Properties

Visualization. To visualize the two finite models, we compute the shift matrices $\phi(x)$ and $\phi(y)$ by letting x and y operate on the respective basis of $\mathcal{M}$. The graph with $\phi(x) + \phi(y)$ as adjacency matrix is the visualization of the finite model and is shown in Fig. 12 for $n = 5$. The inner structure and the left and bottom are the same as in the infinite case (see Fig. 10). The right and upper boundary reflect (27) and (28).

Spectrum and Fourier transform. The spectrum is determined by the solutions of $T_{n,0} = T_{0,n} = 0$. To do so, we use the power forms (44) and (45). Setting in these equations $a = u^n$ and $b = v^n$, we first solve for a and b; the nth roots are then the resulting u and v and can be inserted into (42)

for the result. The desired n^2 pairs of (u, v) are

$$(u_i, v_j) = (\omega_n^i, \omega_{3n}^{1+3j}), \quad 0 \le i, j < n, \tag{32}$$

which determine the zeros $(x_{i,j}, y_{i,j})$ via (42). The spectral decomposition of $\mathcal{M}$ is now a special case of (7).

The Fourier transforms for the two models are accordingly given by $n^2 \times n^2$ matrices, which we call the *discrete triangle transforms (DTT)*[8]. For the T-transform it is given by

$$\mathrm{DTT}_{n\times n} = [T_{k,\ell}(x_{i,j}, y_{i,j})]_{0\le i,j<n, 0\le k,\ell<n}; \tag{33}$$

we call it the DTT of type 1. The double index (i, j) is the row index, and (k, ℓ) is the column index of the matrix, both ordered lexicographically. The exact form is obtained by inserting (32) into the power form of $T_{k,\ell}$ (Table IV in Appendix B): the entry at position $(i, j), (k, \ell)$ is then given by

$$\tfrac{1}{6}\big(\omega_{3n}^{3ki-3\ell j-\ell} + \omega_{3n}^{3kj-3\ell i+k} + \omega_{3n}^{3ki+3\ell i+3\ell j+\ell} + \omega_{3n}^{3\ell i+3kj+3\ell j+k+\ell} + \omega_{3n}^{-3ki-3\ell i-3kj-k} + \omega_{3n}^{-3ki-3kj-3\ell j-k-\ell}\big).$$

The DTT is invertible by construction (see Section II-C), and even "almost" orthogonal as explained below.

The smallest example is $n = 2$. We have $T_{0,0} = 1, T_{0,1} = y, T_{1,0} = x, T_{1,1} = \frac{1}{2}(3xy - 1)$; the zeros of $T_{2,0} = T_{0,2} = 0$, i.e., $3x^2 - 2y = 3y^2 - 2x = 0$, are given by (in this order)

$$(\tfrac{2}{3}, \tfrac{2}{3}), (0, 0), (\tfrac{2}{3}\omega_3, \tfrac{2}{3}\omega_3^2), (\tfrac{2}{3}\omega_3^2, \tfrac{2}{3}\omega_3).$$

Thus, $\mathrm{DTT}_{2\times 2}$ is the 4×4 matrix

$$\mathrm{DTT}_{2\times 2} = \begin{bmatrix} 1 & \frac{2}{3} & \frac{2}{3} & \frac{1}{6} \\ 1 & 0 & 0 & -\frac{1}{2} \\ 1 & \frac{2}{3}\omega_3^2 & \frac{2}{3}\omega_3 & \frac{1}{6} \\ 1 & \frac{2}{3}\omega_3 & \frac{2}{3}\omega_3^2 & \frac{1}{6} \end{bmatrix}.$$

Similarly, we can define a DTT of type 2 by replacing T with U in (33).

It is well-known that the 2-D DFT samples the continuous spectrum associated with the 2-D z-transform in Fig. 11(a) at lattice points $(\alpha_k, \beta_\ell) = (2\pi k/n, 2\pi\ell/n)$, $0 \le k, \ell < n$. Similarly, the DTT (type 1) samples the continuous spectrum associated with the 2-D hexagonal T-transform in Fig. 11(c). The details are shown in Fig. 13. Namely, (32) determines the sampling points in Fig. 13(a) spread over the entire torus in Fig. 11(a), i.e., over all six copies of the triangular spectral domain in Fig. 11(c). To obtain the actual sampling, we map all points into the triangle (Fig. 13(b)) using affine mappings according to the symmetric b.c.'s in Fig. 11(c). The sampling points form a honeycomb pattern, which is best seen by mapping (again in an affine way) the triangle to an equilateral one as shown in Fig. 13(c). For practical applications Fig. 13(c) seems to be a natural choice because the sampling points are evenly distributed. We will show a small application example later in Section VII.

Unitary version and inverse. In Section IV-B we asserted that the DCT and DST of type 3 are almost orthogonal since their visualizations in Fig. 7 are undirected except for the boundary. Using the same argument, we derive a unitary version of the DTT, focusing on type 1.

The adjacency matrix of the visualization in Fig. 12 is, by construction, $\phi(x) + \phi(y)$. Also by construction, the graph is undirected, except for the boundary. The goal is to find an $n^2 \times n^2$-matrix D_{n^2}, such that $D_{n^2}^{-1}(\phi(x) + \phi(y))D_{n^2}$ is symmetric. Then, $\mathrm{DTT}_{n\times n}\, D_{n^2}$ is unitary up to possibly a scaling of the rows. The solution (provided without proof) is

$$D_{n^2} = R_{n^2} \cdot E_{n^2}. \tag{34}$$

Here, R_{n^2} is an orthogonal matrix that applies the rotation $\frac{1}{\sqrt{2}}\mathrm{DFT}_2$ to each pair of input elements with indices $(in + j, (n - j)n + (n - i))$, $1 \le i, j < n$, $i + j \ne n$. There are exactly $\binom{n-1}{2}$ such pairs.

$E_{n^2} = \mathrm{diag}(L)$ is diagonal. The list L is given by the concatenation $\bigcup_{i=0}^{n-1} L_i$, where each L_i has length n. Further, $L_0 = \frac{1}{n}(1, \sqrt{3}, \ldots, \sqrt{3})$, and, for $i = 1, \ldots, n-1$,

$$L_i = \frac{2}{n}\big(\sqrt{3}/2, \underbrace{\sqrt{3}, \ldots, \sqrt{3}}_{n-i}, \underbrace{1, \ldots, 1}_{i-1}\big).$$

No further rescaling of the rows is necessary, i. e., the matrix $\mathrm{DTT}_{n\times n}\, D_{n^2}$ is unitary. In particular,

$$\mathrm{DTT}_{n\times n}^{-1} = D_{n^2}\, \mathrm{DTT}_{n\times n}^{H},$$

since D_{n^2} is real and symmetric; $(\cdot)^H$ denotes the transpose-conjugate of a matrix.

Diagonalization properties. The general theory (Section II-C) establishes that the matrices diagonalized by $\mathrm{DTT}_{n\times n}$ are precisely the matrices $\phi(h(x, y)) = h(\phi(x), \phi(y))$, $h \in \mathcal{A}$. In particular, the adjacency matrix of the visualization (Fig. 12) is diagonalized.

C. Discussion

Signal model versus actual data. The DTT processes an $n \times n$ array, just like the 2-D DFT, any 2-D DCT, or any 2-D transform considered in [10]. In particular, this means that the DTT could be applied to data given on a rectangular lattice. The decision which transformation actually to choose is up to the user and motivates our notion of a signal *model*, which is implicitly imposed by the transform chosen and best understood by its visualization as graph (Fig. 1). Applying a model (via the generalized z-transform Φ) means associating the given discrete data with the nodes of the graph, which implicitly imposes distance relations including the presence of a direction or not. The DTT, and its associated signal model, is designed for images (undirected model) in which each pixel has six neighbors at equal distance and hence should be the replacement for the 2-D DCT if the application at hand satisfies this assumption.

Underlying continuous signal model and sampling. In standard time (i.e., directed) SP, for every discrete signal model there is an underlying continuous model and the models are connected by sampling with an associated sampling theorem. For undirected models, the corresponding theory does not exist to our knowledge. For the DCT, we have recently identified the underlying continuous model and the proper sampling theorem

[8]The name reflects that the hexagonal lattice tessellates the plane into equilateral triangles.

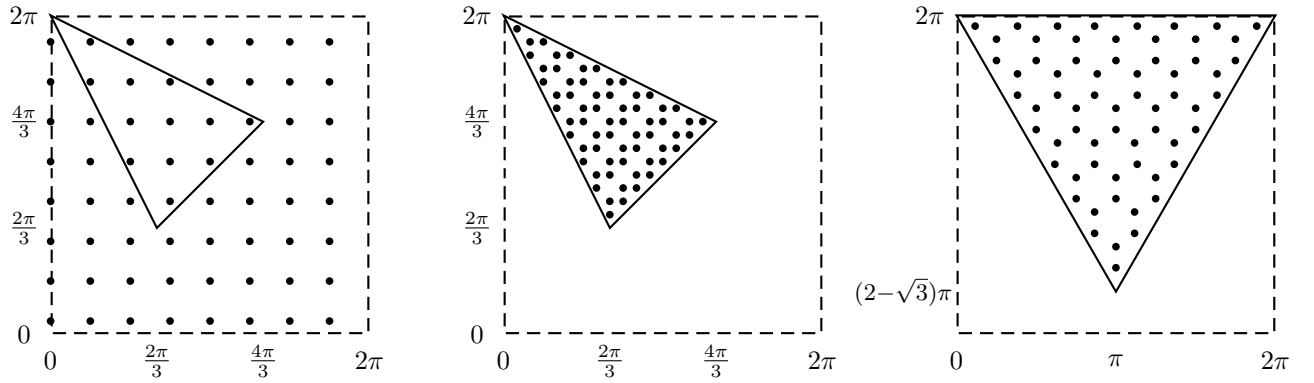

(a) Sampling points determined by (32)

(b) Sampling points mapped into the triangle

(c) Triangle and sampling points in (b) mapped to an equilateral triangle

Fig. 13. The $\mathrm{DTT}_{n\times n}$ samples the spectrum in Fig. 11(c) as illustrated here for $n = 8$.

as part of the algebraic theory [20]. As the discrete model (12) underlying the DCT, also the associated continuous model has a notion of filtering different from the standard convolution.

The derivation of sampling theorems associated with the DTT is still ongoing work. However, it is interesting to note that our derivation of the the discrete models for 1-D time (in [4]), 1-D space (Section III), and 2-D hexagonal space (Section V) is bottom-up and does not require a continuous model as starting point.

Connection to Gauss-Markov random fields. In [3], we established the equivalence (under certain conditions) between shift-invariant finite signal models (in the algebraic theory) and stochastic models given by Gauss-Markov random fields (GMRFs) with proper boundary conditions. In particular, this established the same equivalence between the algebraic notion of Fourier transform and the Karhunen-Loève transforms (KLTs) for these fields. The discussion focused on 1-D models (Section II-B) but is readily extended to the 2-D models here. An extensive treatment exceeds the scope of this paper; we only give an example. Consider the non-causal first-order GMRF defined on the index set $0 \le k, \ell < n$ by

$$s_{k,\ell} = a(s_{k+1,\ell} + s_{k,\ell-1} + s_{k-1,\ell+1}) + b(s_{k,\ell+1} + s_{k-1,\ell} + s_{k+1,\ell-1}) + \nu_{k,\ell},$$

where the $s_{i,j}$ are random variables, a, b real constants, and $\nu_{k,\ell}$ zero-mean Gaussian noise. Then the unitary DTT, i. e., the 2-D transform given by $\mathrm{DTT}_{n\times n}\, D_{n^2}$, is a KLT for these fields if proper boundary conditions, determined by the model (31), are chosen.

On the signal extension found. We asserted above that the signal models (31) have no monomial signal extension. This seems to be an inherent property of the hexagonal lattice: each node has six neighbors; in particular, each node at the boundary of Fig. 12 has two edged going outwards in contrast to one edge for the separable models (Figs. 1(a) and (b)).

Summary of signal models. Table I summarizes all finite 2-D signal models considered in this paper. In each case, there is a corresponding infinite model. The last column contains the new models for the spatial hexagonal lattice.

Fig. 14. 200×200 image of some leaves used for the experiment.

VII. Application to an Image

In this section we give an example for applying the 2-D DCT and the DTT to an image. The goal is to show basic similarities and differences. A detailed quantitative study is future work. In both cases we use the unitary version of the transform, i.e., the total energy is preserved.

For the experiment we use the 200×200 gray-scale 8-bit image of some leaves shown in Fig. 14.

First, we assume the space model for the finite 2-D T-transform (i.e., we impose the structure in Fig. 1(b)) and hence apply the 2-D DCT to compute the spectrum. The magnitude spectrum is displayed in Fig. 15(a). This spectrum regularly samples the continuous spectrum associated with the infinite 2-D T-transform (the gray area in Fig. 11(b)). The bottom left corner in Fig. 15(a) represents the low frequencies.

Second, we assume the space model given by the finite 2-D hexagonal T-transform (i.e., we impose the structure in Fig. 1(c), which inherently distorts the image) and hence compute the spectrum using the DTT. The magnitude spectrum is shown in Fig. 15(b) and corresponds to Fig. 13(a). To properly display the spectrum we map all coefficients to the triangle in Fig. 15(c), which corresponds to Fig. 13(c). The low

TABLE I
2-D SIGNAL MODELS DISCUSSED IN THIS PAPER. THE LAST COLUMN CONTAINS THE NEW MODEL DERIVED FOR 2-D HEXAGONAL SPACE. ONLY THE FINITE MODELS ARE SHOWN (THE COMMON WORD "FINITE" IN THE ROW FOR Φ IS OMITTED) AND ONLY TWO OUT OF THE SIXTEEN FINITE SPACE MODELS, NAMELY THOSE WHICH HAVE A 2-D HEXAGONAL COUNTERPART.

	2-D time (separable)	2-D space (separable)	2-D hexagonal space
$\mathcal{A} = \mathcal{M}$	$\mathbb{C}[x,y]/\langle x^n-1, y^n-1\rangle$	$\mathbb{C}[x,y]/\langle T_n(x), T_n(y)\rangle$	$\mathbb{C}[x,y]/\langle T_{n,0}(x,y), T_{0,n}(x,y)\rangle$
Φ	2-D z-transform	2-D T,U-transform	2-D hexagonal T,U-transform
$\mathcal{F}$	$\mathrm{DFT} \otimes \mathrm{DFT}$	$\mathrm{DCT} \otimes \mathrm{DCT}, \mathrm{DST} \otimes \mathrm{DST}$ type 3	DTT type 1 and 2
Visualization	Fig. 1(a)	Fig. 1(b)	Fig. 12

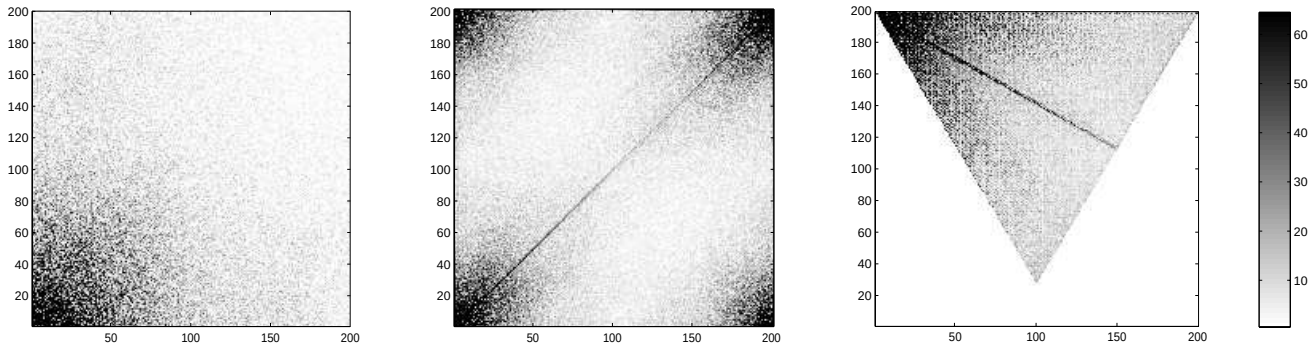

(a) 2-D DCT spectrum (b) 2-D DTT spectrum (raw data) (c) 2-D DTT spectrum

Fig. 15. Magnitude spectra of the image in Fig. 14 with respect to the finite 2-D space model and the finite 2-D hexagonal space model.

frequencies are in the upper left corner. The common intensity scale for all plots in Fig. 15 is on the far left. We note that a few values much higher than 60 occur in all spectra.

We observe the energy compaction around the low frequencies for both transforms. The triangle appears somewhat darker since the same energy is displayed on less space. The line crossing the spectrum of the DTT is not due to the image but seems to be an inherent property of the transform.

VIII. CONCLUSIONS

We derived a novel SP framework for the 2-D spatial hexagonal lattice. The derivation is based on the algebraic theory of signal processing and, we believe, provides an example of the usefulness of this theory. Namely, it not only yields the proper spectral transform DTT, but the full set of associated basic SP concepts including convolution, "z-transform," transform properties, and fast algorithms [6], [8]. Further, the theory shows the precise analogy to the DCTs and DSTs, which is of theoretical interest, but also immediately makes the DTT a candidate for hexagonal image processing applications such as robotics vision, deep-space imaging, or biomedical imaging.

Finally, we note that the relationship between Chebyshev polynomials in two variables and polynomial algebras and the hexagonal lattice is not standard in mathematics and provides insights that are not contained in the classic mathematical literature (such as [19], [21]).

ACKNOWLEDGMENT

The authors would like to thank Aliaksei Sandryhaila for helping with the image experiment.

REFERENCES

[1] G. Strang, "The discrete cosine transform," *SIAM Review*, vol. 41, no. 1, pp. 135–147, 1999.
[2] M. Püschel and M. Rötteler, "The discrete triangle transform," in *Proc. ICASSP*, 2004, vol. 3, pp. 45–48.
[3] M. Püschel and J. M. F. Moura, "Algebraic signal processing theory," available at http://arxiv.org/abs/cs.IT/0612077, parts of this manuscript are submitted as [4] and [5].
[4] M. Püschel and J. M. F. Moura, "Algebraic signal processing theory: Foundation and 1-D time," submitted for publication, part of [3].
[5] M. Püschel and J. M. F. Moura, "Algebraic signal processing theory: 1-D space," submitted for publication, part of [3].
[6] M. Püschel and M. Rötteler, "Cooley-Tukey FFT like algorithm for the discrete triangle transform," in *Proc. 11th IEEE DSP Workshop*, 2004, pp. 158–162.
[7] M. Püschel and J. M. F. Moura, "Algebraic signal processing theory: Cooley-Tukey type algorithms for DCTs and DSTs," submitted for publication.
[8] M. Püschel and M. Rötteler, "Algebraic signal processing theory: Cooley-Tukey type algorithms on the 2-D hexagonal spatial lattice," submitted for publication.
[9] R. M. Mersereau, "The processing of hexagonally sampled two-dimensional signals," *Proceedings of the IEEE*, vol. 67, no. 6, pp. 930–949, 1979.
[10] D. E. Dudgeon and R. M. Mersereau, *Multidimensional Digital Signal Processing*, Prentice-Hall, 1984.
[11] A. M. Grigoryan, "Hexagonal discrete cosine transform for image coding," *IEEE Transactions on Signal Processing*, vol. 50, no. 6, pp. 1438–1448, 2002.
[12] I. Her, "Geometric transformation on the hexagonal grid," *IEEE Transactions on Image Processing*, vol. 4, no. 9, pp. 1213–1222, 1995.

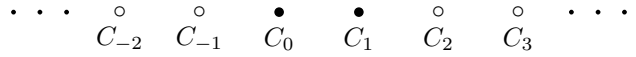

Fig. 16. The entire two-sided sequence of Chebyshev polynomials is uniquely determined by the initial conditions C_0 and C_1 (solid bullets) via (35).

[13] D. Van de Ville, T. Blu, M. Unser, W. Philips, I. Lemahieu, and Rik Van deWalle, "Hex-splines: A novel spline family for hexagonal lattices," *IEEE Transactions on Image Processing*, vol. 13, no. 6, pp. 758–772, 2004.

[14] R. Ulichney, *Digital Halftoning*, MIT Press, 1987.

[15] L. Middleton and J. Sivaswamy, *Hexagonal Image Processing*, Springer, 2005.

[16] H.-S. Wu, "Hexagonal discrete cosine transform for image coding," *Electronics Letters*, vol. 27, no. 9, pp. 781–783, 1991.

[17] H. J. Nussbaumer, *Fast Fourier Transformation and Convolution Algorithms*, Springer, 2nd edition, 1982.

[18] D. Cox, J. Little, and D. O'Shea, *Ideals, Varieties, and Algorithms*, Springer, 1997.

[19] T. Koornwinder, "Orthogonal polynomials in two variables which are eigenfunctions of two algebraically independent partial differential operators (part III)," *Indag. Math.*, vol. 36, pp. 357–369, 1974.

[20] J. Kovacevic and M. Püschel, "Sampling theorem associated with the discrete cosine transform," in *Proc. ICASSP*, 2006.

[21] R. Eier and R. Lidl, "A class of orthogonal polynomials in k variables," *Math. Ann.*, vol. 260, pp. 93–99, 1982.

[22] T. S. Chihara, *An Introduction to Orthogonal Polynomials*, Gordon and Breach, 1978.

APPENDIX A
CHEBYSHEV POLYNOMIALS IN ONE VARIABLE

Chebyshev polynomials, and the more general class of orthogonal polynomials, have many interesting properties and play an important role in different areas of mathematics, including statistics, approximation theory, and graph theory. An excellent introduction to the theory of orthogonal polynomials can be found for example in the book of Chihara [22]. In this section we give the main properties of Chebyshev polynomials that we will use in this paper.

Definition through recurrence. We call every sequence $C = (C_n(x) \mid n \in \mathbb{Z})$ of polynomials that satisfies the three-term recurrence

$$C_{n+1} = 2xC_n - C_{n-1} \tag{35}$$

a sequence of *Chebyshev polynomials* (C stands for Chebyshev). In (35), C_{n+1} and C_{n-1} can be swapped, which means the recurrence can be run in both directions. Hence, the entire sequence C is uniquely determined by any two consecutive polynomials, usually the initial polynomials C_0, C_1 (see Fig. 16). In this paper, we require $C_0 = 1$ and that C_1 is of degree 1. Consequently, C_n, $n \geq 0$ is of degree n. This implies that only the C_n, $n \geq 0$ are linearly independent.

First and second kind. The most important—and commonly known—are the Chebyshev polynomials of the first and second kind, denoted with $C = T$ and $C = U$, respectively. Table II shows the two sequences around $n = 0$.

The Chebyshev polynomials T_n can be written in a parameterized form, called power form, as

$$T_n = \frac{1}{2}(u^n + u^{-n}), \quad x = \frac{1}{2}(u + u^{-1}). \tag{36}$$

For $x \in [-1, 1]$, we can substitute $u = e^{j\theta}$ and get the trigonometric form

$$T_n = \cos n\theta, \quad \cos\theta = x. \tag{37}$$

TABLE II
CHEBYSHEV POLYNOMIALS OF THE FIRST AND SECOND KIND FOR SMALL VALUES OF n.

	$n=-3$	-2	-1	0	1	2	3
$C=T$	$4x^3-3x$	$2x^2-1$	x	1	x	$2x^2-1$	$4x^3-3x$
U	$-2x$	-1	0	1	$2x$	$4x^2-1$	$8x^3-4x$

Both parameterizations exhibit the *symmetry property*

$$T_{-n} = T_n. \tag{38}$$

The form (37) can be used to readily derive the zeros of T_n.

Similar properties hold for the Chebyshev polynomials of the second, third, and fourth kind, denoted by U_n, V_n, W_n, respectively, that arise from different initial polynomials C_0, C_1. They are summarized in Table III.

There are also numerous relationships between Chebyshev polynomials of different kinds. We will use only

$$T_n = \frac{1}{2}(U_n - U_{n-2}). \tag{39}$$

In addition, we will need the following property that is shared by all sequences of Chebyshev polynomials including T and U (see [22]).

Lemma 2 Let $C = (C_n \mid n \in \mathbb{Z})$ be a sequence of Chebyshev polynomials. Then

$$T_k \cdot C_n = \frac{1}{2}(C_{n+k} + C_{n-k}).$$

APPENDIX B
CHEBYSHEV POLYNOMIALS IN TWO VARIABLES

The Chebyshev polynomials in two variables are far lesser known than their univariate counterparts. Several different definitions exist in the literature; we use the one in [19] with minor modifications. The presentation is different from [19] and chosen to parallel Appendix A.

By abuse of notation, we will use, as for one variable, the letters C, T, U to denote general Chebyshev polynomials, and those of first and second kind respectively.

The presentation is chosen to parallel as much as possible Appendix A and to motivate why they provide the underpinning of the hexagonal space model derived in this paper.

Definition through recurrence. The general Chebyshev polynomials in two variables are an array of polynomials $C = (C_{m,n}(x, y) \mid m, n \in \mathbb{Z})$ best visualized as arranged in a hexagonal 2-D array indexed with m and n as shown in Fig. 17. The reason for the hexagonal structure is in the two defining recurrence equations:

$$C_{m+1,n} = 3xC_{m,n} - C_{m,n-1} - C_{m-1,n+1}, \tag{40}$$
$$C_{m,n+1} = 3yC_{m,n} - C_{m-1,n} - C_{m+1,n-1}. \tag{41}$$

In both equations we can, as in the one variable case, swap polynomials to run the recurrence in different directions. The four polynomials in (40) are $C_{m,n}$ and three of its six neighbors: right, upper left, lower left. The other three

TABLE III
TWO SERIES OF CHEBYSHEV POLYNOMIALS. THE RANGE FOR THE ZEROS IS $0 \le k < n$. IN THE TRIGONOMETRIC FORM $\cos\theta = x$ AND IN THE POWER FORM $x = (u + u^{-1})/2$.

polynomial	$n = 0, 1$	trigonometric form	power form	symmetry	zeros
T_n	$1, x$	$\cos(n\theta)$	$\frac{u^n+u^{-n}}{2}$	$T_{-n} = T_n$	$\cos\frac{(k+\frac{1}{2})\pi}{n}$
U_n	$1, 2x$	$\frac{\sin(n+1)\theta}{\sin\theta}$	$\frac{u^{n+1}-u^{-(n+1)}}{u-u^{-1}}$	$U_{-n} = -U_{n-2}$	$\cos\frac{(k+1)\pi}{n+1}$

TABLE IV
TWO SERIES OF CHEBYSHEV POLYNOMIALS IN TWO VARIABLES. IN THE POWER FORM $x = (u + v + (uv)^{-1})/3$, $y = (u^{-1} + v^{-1} + uv)/3$ AND $c^{\pm}_{m,n}(u, v) = u^n v^{-m} \pm u^{-m} v^n \pm u^{n+m} v^m + u^m v^{n+m} + u^{-n-m} v^{-n} \pm u^{-n} v^{-n-m}$.

polynomial	$(m, n) =$ $(0,2), (0,1), (1,1)$ $(0,0), (1,0), (2,0)$	power form	symmetry
$T_{m,n}$	$3y^2 - 2x, y, (3xy - 1)/2$	$\frac{1}{6}c^{+}_{m,n}(u, v)$	$T_{-m,n} = T_{m,n-m}$
	$1, x, 3x^2 - 2y$		$T_{m,-n} = T_{m-n,n}$
$U_{m,n}$	$9y^2 - 3x, 3y, 9xy - 1$	$c^{-}_{m+1,n+1}(u, v)/c^{-}_{1,1}(u, v)$	$U_{-m,n} = -U_{m-2,n-m+1}$
	$1, 3x, 9x^2 - 3y$		$U_{m,-n} = -U_{m-n+1,n-2}$

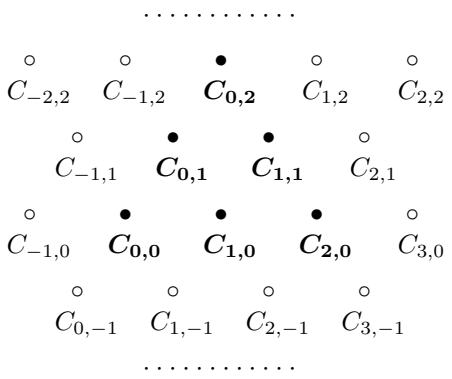

Fig. 17. The entire 2-D array of Chebyshev polynomials in two variables is uniquely determined by the initial conditions $C_{0,0}$, $C_{1,0}$, $C_{2,0}$, $C_{0,1}$, $C_{1,1}$, $C_{0,2}$ (solid bullets) via (40) and (41).

neighbors are in (41). The obtained structure is equivalent to the two hexagonal space shifts in Fig. 8.

The entire array C is uniquely determined by the six initial polynomials shown in Fig. 17. Again, we require $C_0 = 1$. For the other five initial polynomials $C_{i,j}$ we require that a) $C_{i,j}$ has total[9] degree $i + j$; b) only one summand $cx^a y^b$ of $C_{i,j}$ has $a + b = i + j$ and $a = i, b = j$.

With these conditions for the six initial polynomials we have the following lemma on the array of all $C_{m,n}$.

Lemma 3 Every polynomial $C_{m,n}$ has total degree $m + n$. Further, only one summand $cx^a y^b$ has $a + b = m + n$ and for this summand $a = m$ and $b = n$. As a consequence, the polynomials $\{C_{m,n} \mid m, n \ge 0\}$ are a basis of $\mathbb{C}[x, y]$.

As in the one variable case, this lemma implies that every polynomial $C_{m,n}$ with $m < 0$ or $n < 0$ is a linear combination of Chebyshev polynomials in the positive quadrant.

[9]The total degree of $p(x, y)$ is the largest $a + b$ over all summands $cx^a y^b$ of p.

This determines the symmetry properties of C, and in the signal processing context the associated boundary condition and signal extension.

First and second kind. The Chebyshev polynomials (in two variables) of the first and second kind are defined through the initial conditions shown in Table IV. The same table shows the power forms in both cases, a u, v-parameterization with

$$x = \frac{1}{3}(u + v + (uv)^{-1}),\ y = \frac{1}{3}(u^{-1} + v^{-1} + uv). \quad (42)$$

Substituting $u = e^{j\phi}$, $v = e^{j\psi}$ yields the trigonometric form, which cannot be further simplified, unlike as in the one variable case.

We did not find, nor were we able to derive, suitable Chebyshev polynomials of the third and fourth kind in two variables.

The equivalent of (39) is the property

$$T_{n,0} = \frac{1}{3}(U_{n,0} - U_{n-2,1} + U_{n-3,0}), \quad (43)$$

which can be confirmed using the respective power forms.

The following lemma is the equivalent of Lemma 2. We omit the proof, which is by induction and straightforward.

Lemma 4 Let $C = (C_{m,n} \mid m, n \in \mathbb{Z})$ be an array of Chebyshev polynomials in two variables. Then

$$T_{k,\ell} \cdot C_{m,n} = \frac{1}{6}(C_{m-k-\ell,n+k} + C_{m-k,n+k+\ell} + C_{m+k,n+\ell} + C_{m+k+\ell,n-\ell} + C_{m+\ell,n-k-\ell} + C_{m-\ell,n-k})$$

Further properties and notation. The following properties and notation makes it simpler to compute with Chebyshev polynomials in two variables. If $p(x, y) \in \mathbb{C}[x, y]$, then we denote with $\overline{p}(y, x)$ the same polynomial with exchanged variables.

For $C_{m,n}(x, y)$, exchanging x and y is equivalent to replacing u, v by u^{-1}, v^{-1} in the power form (Table IV). Evaluation

shows that for $C = T, U$,

$$\overline{C}_{m,n}(x, y) = C_{n,m}(x, y).$$

Setting $C_{m,0} = C_m$ (not to be confused with the Chebyshev polynomials in one variable), this implies $C_{0,n} = \overline{C}_n$. Using again the power forms we can now establish

$$T_{m,n} = \frac{1}{2}(3T_m\overline{T}_n - T_{m-n}),$$
$$U_{m,n} = U_m\overline{U}_n - U_{m-1}\overline{U}_{n-1}.$$

Further, the power forms of T_n and $\overline{T}_n$ have only three summands:

$$T_n = T_{n,0} = \frac{1}{3}(u^n + v^n + (uv)^{-n}), \tag{44}$$

$$\overline{T}_n = T_{0,n} = \frac{1}{3}(u^{-n} + v^{-n} + (uv)^n). \tag{45}$$

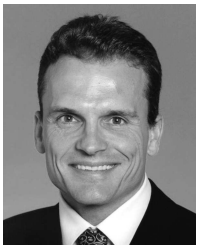

Markus Püschel is an Associate Research Professor of Electrical and Computer Engineering at Carnegie Mellon University. He received his Diploma (M.Sc.) in Mathematics and his Doctorate (Ph.D.) in Computer Science, in 1995 and 1998, respectively, both from the University of Karlsruhe, Germany. From 1998-1999 he was a Postdoctoral Researcher at Mathematics and Computer Science, Drexel University. Since 2000 he has been with Carnegie Mellon University. He is an Associate Editor for the IEEE Transactions on Signal Processing, and was an Associate Editor for the IEEE Signal Processing Letters, a Guest Editor of the Journal of Symbolic Computation, and the Proceedings of the IEEE. His research interests include signal processing theory/software/hardware, scientific computing, compilers, applied mathematics and algebra.

Martin Rötteler was born in Mannheim, Germany, in 1972. He received the Diploma degree in computer science in 1997 and the Ph.D. degree in 2001, both from the University of Karlsruhe, Germany. From 2003–2004 he was a post-doctoral fellow with the Department of Combinatorics and Optimization and the Institute for Quantum Computing, University of Waterloo, Canada. Since January 2005, he is a research staff member at NEC Laboratories America, Princeton, U.S.A., where he is a member of the Quantum IT group. His research interests include quantum algorithms, quantum error-correcting codes, and signal processing.